RELATIVISTIC CALCULATION OF TRANSITION PROBABILITIES FOR 557.7 nm AND 297.2 nm EMISSION LINES IN OXYGEN

C. T. CHANTLER[1], T. V. B. NGUYEN[1], J. A. LOWE[1], AND I. P. GRANT[2]
[1] School of Physics, University of Melbourne, Australia; chantler@unimelb.edu.au
[2] Mathematical Institute, Oxford University, Oxford, UK

ABSTRACT

The 557.7 nm green line and the 297.2 nm ultraviolet line in oxygen have been studied extensively due to their importance in astrophysics and atmospheric science. Despite the enormous effort devoted to these two prominent transition lines over 30 years, and in fact going back to 1934, the ratio of their transition probabilities remains a subject of major discrepancies amongst various theoretical calculations for many decades. Moreover, theoretical results are inconsistent with available laboratory results, as well as recent spacecraft measurements of Earth's airglow. This work presents new relativistic theoretical calculations of the transition probabilities of these two photoemission lines from neutral oxygen using the multi-configuration Dirac–Hartree–Fock method. Our calculations were performed in both length and velocity gauges in order to check for accuracy and consistency, with agreement to 8%. Whilst remaining a challenging computation, these results directly bear upon interpretations of plasma processes and ionization regimes in the universe.

Key words: atmospheric effects – atomic processes – line: identification – methods: analytical – radiation mechanisms: general – techniques: spectroscopic

Online-only material: color figure

1. INTRODUCTION

Oxygen is one of the most abundant elements in the universe, and as a result exists in many astronomical objects. The oxygen spectra observed contain emission lines from both the visible and non-visible (infrared and ultraviolet). Two of the most prominent lines observed in Earth's aurorae and airglow are the 557.7 nm visible green line and the 297.2 nm ultraviolet line. Moreover, the O I forbidden green line has also been identified in planetary nebulae and meteors such as Perseid, Orionid, and Lyrid (Halliday 1960). This allows further investigations into meteor compositions and the chemical processes involved, which is important for prebiotic studies (Jenniskens & Stenbaek-Nielsen 2004). Furthermore, this green line is believed to be the primary source of luminosity of the Leonid persistent train, which enables the investigation of meteoric aerothermal chemistry (Jenniskens et al. 2000). The auroral green line also features prominently in many young, oxygen-rich supernova remnants such as Cas A, G298 + 1.8, and N132D (Victor et al. 1994), as well as T Tauri stars (Pascucci et al. 2011).

Due to the correlation between forbidden line emission and disk accretion in classical T Tauri stars (Hartigan et al. 1995), information on mass-loss rate and mass accretion rate can also be obtained using this auroral green line. Modeling of atomic processes in comets such as the C/1996 B2 Hyakutake has also been based on this green emission line (Bhardwaj & Raghuram 2012). However, these studies depend upon the transitions following the relevant model which they are presenting, which has not thus far been possible. A major achievement of recent time is the detection of the 5577 auroral green line on Venus (Slanger et al. 2001), which serves as a stepping stone toward a better understanding of the dynamics of its upper atmosphere (Witasse & Nagy 2006). The auroral green line is particularly sensitive to solar and geomatic activities (Russell 1981), so the intensity variation of this emission line can be used for studies of solar flare (Kudryashev & Avakyan 2000), the atmospheric

system, and geophysical disturbances (Mikhalev 2011). Interest in these particular transition lines, especially the auroral green line, is not confined only to astrophysics and plasma physics, but is also important in other areas such as climatology and aeronomy (Semenov & Shefov 2005; Shefov et al. 2000; Semenov et al. 2002; Mikhalev 2012).

Accurate determination of emission lines transition probabilities is especially important, as it can lead to the deduction of the underlying chemical reactions and therefore a better understanding of the evolution of the associated entity. The auroral green line has been a subject of debate for many decades, particularly arising from the disagreement between theoretical calculations and observations. This anomaly has been encountered in studies of electron energy loss in oxygen plasmas (Victor et al. 1994), oxygen UV airglow (Stegman & Murtagh 1988), quantum yields in the nocturnal F-region (Bates 1992), and supernovae (Ryder et al. 1993).

The 557.7 nm visible green line results from the electric quadrupole ($E2$) transition $1s^2\,2s^2\,2p^4(^1S_0-^1D_2)$, which is optically forbidden. The 297.2 nm ultraviolet line is a magnetic dipole ($M1$) transition $1s^2\,2s^2\,2p^4(^1S_0-^3P_1)$. The intensity ratio $I_{557.7}/I_{297.2} = A_{557.7}/A_{297.2}$ of these two lines (or equivalently, the transition probability ratio) has been calculated many times previously by a range of authors but without agreement (Table 1). Note that experiments can report either photon-counting ratios corresponding to $A_{557.7}/A_{297.2}$ or energy-deposition ratios (erg s^{-1}, etc.) but that all data reported here follows the photon-counting standard.

Two laboratory measurements were performed by McConkey et al. (1966) and LeBlanc et al. (1966). Their results are given in Table 2. The theoretical results do not agree with each other, and do not agree well with those from available laboratory measurements. The most recent measurements of this intensity ratio are sourced from the Earth's airglow (Table 3). Interestingly, these recent measurements are quite consistent with each other, and yet disagree strongly with those from

Table 1
List of Various Theoretical Results for the Intensity Ratio $I_{557.7}/I_{297.2}$, Along with the National Institute of Standards and Technology (NIST) Recommended Theoretical Value

Theoretical Calculations	$I_{557.7}/I_{297.2}$
Condon (1934)	11.1
Pasternack (1940)	24.4
Garstang (1951)	16.4
Yamanouchi & Horie (1952)	30.4
Garstang (1955)	17.6
Froese-Fischer & Saha (1983)	13.6
Baluja & Zeippen (1988)	15.9
Galavis et al. (1997)	14.2
Fischer & Tachiev (2004)	16.1
NIST recommendation	16.7

Note. Clearly, there are major discrepancies amongst all the published computations performed thus far.

Table 2
Laboratory Results of the $I_{557.7}/I_{297.2}$ Ratio

Observations/Measurements	$I_{557.7}/I_{297.2}$
McConkey et al. (1966)	18.6 ± 3.7
LeBlanc et al. (1966)	22 ± 2

Table 3
Various Spacecraft Measurements of the Earth's Airglow of the Intensity Ratio $I_{557.7}/I_{297.2}$, and the Average Measured Value

Observations/Measurements	$I_{557.7}/I_{297.2}$
Sharp & Siskind (1989)	9
Slanger et al. (2006)	9.8 ± 1.0
Gattinger et al. (2009)	9.3 ± 0.5
Gattinger et al. (2010)	9.5 ± 0.5
Average	9.4 ± 1.0

Note. These measurements are quite consistent with each other, but disagree with all the available theories listed in Table 1.

the laboratory measurements. Of course, the reason for using this ratio to calibrate the system and the spectra is because the upper level is common, implying that whatever population mechanism might be involved, the intensity ratios should correspond to the ratio of *A*-coefficients. So this is an anomaly. A possible explanation for this discrepancy is the density of the environment in which these measurements were taking place. In particular, a molecular band is seen to be near the green line. While in early measurements this was a problem of detector resolution, later experiments claimed that this was fully addressed and yet the anomaly remained.

The recent observational measurements of the intensity ratio $I_{557.7}/I_{297.2}$ are quite consistent with each other although they are dramatically different from all previous theoretical measurements. Investigating the discrepancies amongst theoretical calculations, and those between theory and observations, is the main objective for this work.

Here, the transition probabilities of the 557.7 nm and 297.2 nm transition lines in oxygen are calculated using the multi-configuration Dirac–Hartree–Fock (MCDHF) method using GRASP2K—the General-purpose Relativistic Atomic Structure Package 2000 (Jonsson et al. 2007). Calculations were performed in both the length and velocity gauges so that accuracy could be monitored through gauge convergence.

This is an effective technique which models the completeness of the wavefunction for upper and lower states of a transition across different effective radial or orbital ranges. The convergence of the technique has been proven to successfully model characteristic X-ray transitions in complex open-shell transition metals (Chantler et al. 2009; Lowe et al. 2011, 2010). The greatest success of this approach has been the ab initio modeling of satellite and shake processes in the impact approximation regime for copper and titanium X-ray transitions (Chantler et al. 2012).

2. THEORY

The energy depends upon the (a priori unknown) electronic configuration, which is described by the linear combination of Slater determinants. Linear combinations of Slater determinants of atomic orbitals that are also simultaneous eigenfunctions of the angular momentum operator **J** and parity operator **P** are called configuration state functions (CSF) Φ. However, each electronic configuration characterizes a state of the system which is not an eigenstate of the *N*-electron

Hamiltonian (in whatever model one is using) so that one gets only an approximate system eigenstate by making a linear combination of CSFs with the same symmetry. The relativistic atomic wavefunction, Ψ—sometimes referred to as the approximate or atomic state function (ASF)—is a linear combination of CSFs,

$$\Psi(\Gamma P J M) = \sum_q c_q \, \Phi(\gamma_q P J M), \qquad (1)$$

where γ_q represents all the information required to represent the CSF uniquely, such as orbital occupation/quantum numbers, seniority numbers, etc., and c_q are the mixing coefficients. The CSFs are built from a basis of one-electron Dirac orbitals, while the mixing coefficients can be obtained by diagonalizing the Hamiltonian. In this theory, it is the Dirac–Coulomb Hamiltonian:

$$H_{\rm DC} = \sum_i^N c \, \boldsymbol{\alpha}_i \cdot \boldsymbol{p}_i + \beta_i m c^2 + V_{\rm nuc}(r_i) + \sum_{i<j}^N \frac{1}{r_{ij}}, \qquad (2)$$

where the first summation is the Dirac Hamiltonian with the usual matrix notation, and the second summation is the Coulomb term, with r_{ij} the distance between electron *i* and electron *j*. This process of finding the mixing coefficient is often referred to as *configuration interaction* (CI). As part of our relativistic CI calculations, transverse photon interaction was included in the Hamiltonian, and self-energy correction and vacuum polarization were also accounted for.

3. COMPUTATION

The electronic configurations were obtained through excitations of one or two electrons from the reference configuration ($1s^2 \, 2s^2 \, 2p^4$) into an active set of orbitals (Figure 1). This generates additional CSFs, which effectively contribute to a better approximation of the ASF. Two excitations allows correction for deficiencies within the radial wavefunction and to account for electron–electron correlation. Any triple excitations (or higher) would account for electron–electron–electron correlation, which is a higher-order effect and therefore extremely small.
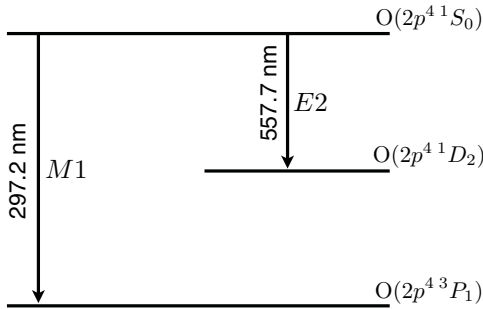
Figure 1. The electric quadrupole ($E2$) and magnetic dipole ($M1$) transitions of interest.

Table 4
Summary of Results for Method A

	$E2$
Transition energy (eV)	2.242 36 (0.01%)
A^L (s^{-1})	1.298 41 (0.04%)
A^V (s^{-1})	0.978 13 (0.48%)
A^V/A^L	0.753
	$M1$
Transition energy (eV)	4.232 85 (0.009%)
A (s^{-1})	0.082 47 (0.03%)
$I_{557.7}/I_{297.2}$ (length)	15.7443 (0.001%)
$I_{557.7}/I_{297.2}$ (velocity)	11.8607 (0.450%)

Notes. Numbers in parentheses are the fluctuation from the earlier cycle. The fluctuation given in parentheses is the percentage difference between the current and immediate previous expansion.

Table 5
Summary of Results for the Optimized Method B

	$E2$
Transition energy (eV)	2.211 55 (0.005%)
Wavelength (nm)	560.622 (0.005%)
A^L (s^{-1})	1.217 85 (0.184%)
A^V (s^{-1})	1.118 85 (2.287%)
A^V/A^L	0.919
	$M1$
Transition energy (eV)	4.198 012 (0.0005%)
Wavelength (nm)	295.340 (0.0005%)
A (s^{-1})	0.078 766 (0.001%)
$I_{557.7}/I_{297.2}$ (length)	15.46 (0.194%)
$I_{557.7}/I_{297.2}$ (velocity)	14.20 (2.254%)

Notes. The fluctuation given in parentheses is the percentage difference between the $n = 11$ and $n = 12$ expansion. The most accurate and stable result appears to be A^L with ratio 15.46 ± 0.03.

Our method (Chantler et al. 2010) involves sequentially expanding the reference configuration by the principal quantum number n (shell). That is, we first added the $3s\,3p\,3d$ orbital, then $4s\,4p\,4d\,4f$, etc. It is often essential to expand by the angular momentum number l (subshell) to achieve convergence for wavefunctions. However, we already have a high-quality wavefunction and faster relaxation from the code. In addition, we also employed the frozen core approximation, so that the inner-shell atomic orbitals are sequentially "frozen" as more outer orbitals are added. That is, initially the core orbitals are allowed to optimize independently, but each time an extra orbital
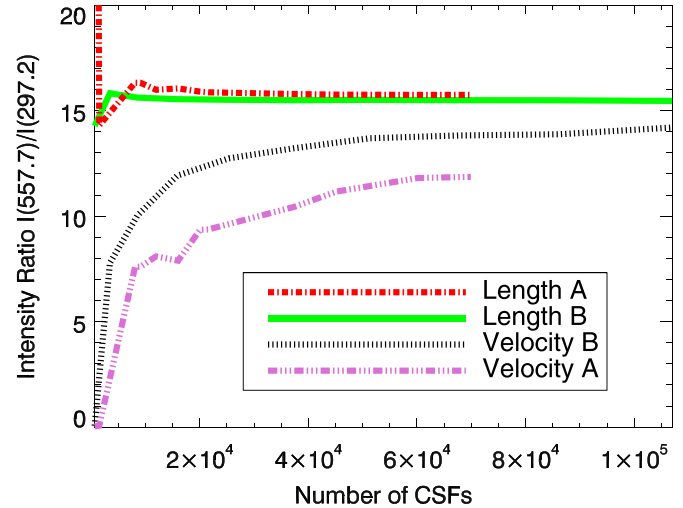

Figure 2. A comparison of gauge convergence using alternative computational Methods A and B. Length and velocity refers to the two different gauges employed for the calculations. A much smoother and faster convergence between the length and velocity gauges can be achieved using Method B.

(A color version of this figure is available in the online journal.)

Table 6
Results for the Last Few Expansions using Method B

n	CSFs	A^V	A^L	$A(M1)$
10	67 599	1.08872	1.22053	0.0787672
11	86 171	1.09326	1.22009	0.0787668
12	106 995	1.11885	1.21785	0.0787660

is added on the outside, the inner orbital is then held fixed so that now only the outer orbital is allowed to be optimized. This method also allows for excitations from any subshell of the reference configuration except for $1s^2$. While each such $1s$-excited CSF has an enormously different eigenvalue from the intended true wavefunction, the percentage contribution in an optimized ASF is extremely small (e.g., 10^{-6}).

4. RESULTS

A preliminary approach was developed, labeled Method A, for performing the relativistic computations. Method A (Table 4) involves expansion by subshell with excitations from $1s^2$ included. Method B is the preferred technique which involves expansion by shell with no excitations from $1s^2$ (Table 5). We have made several specifications of the expansion technique, namely expanding by shell instead of subshell and neglecting excitations from $1s^2$. For our optimized Method B, we have expanded the basis set to the $n = 12$ shell, which contains about 107,000 CSFs. The fluctuation, given inside parentheses in Table 5, is the percentage difference between the current expansion ($n = 12$) and the immediate prior expansion ($n = 11$). A small fluctuation serves as an indicator that the results are stabilizing. The results of the last few expansions for Method B are presented in Table 6.

Results are extremely stable. The length and velocity gauges agree to 8%, as indicated by the ratio A^V/A^L. Figure 2 is a comparison of gauge convergence between two different expansion techniques. The intensity ratio $I_{557.7}/I_{297.2}$ is the ratio between the Einstein A coefficients in $E2$ and $M1$ as presented in the careful observations and measurements. A smoother and faster convergence is obtained using

Table 7
Measured Wavelengths and Transition Energies for the Green ($E2$) and
Ultraviolet ($M1$) Lines According to Moore (1993),
the Current Accepted Values on the NIST Database

	Transition Energy (eV)	Wavelength (nm)
$E2$	2.222 38	557.889
$M1$	4.189 75	295.923

Method B, and the two gauges agree much better following Method B in comparison with Method A. This is a statement of the convergence and completeness of the wavefunctions following a particular approach—that is, that the incorporation of relaxation by shell yields a more uniform convergence of the wavefunction, and hence a more complete description of the excited and ground states. Method A is consistent with results from the more optimized Method B, but with a relatively poor convergence and hence larger uncertainty.

Comparing Tables 4 and 5 and Figure 2 demonstrates that Method B provides much better results in terms of stability and gauge convergence. Energy accuracy is also a useful marker. For the $M1$ transition, the theoretical transition energy for Method B is within about 0.2% of the measured energy as given in Table 7. On the other hand, with Method A the difference is about 1%. Similarly for the $E2$ transition, the theoretical transition energy of Method B is within about 0.5% of the measurement, whereas with Method A it is about 0.9%. Eigenenergies are fairly robust and stable.

The discussion of the origin of gauge discrepancy is beyond the scope of this paper. Past work by our group converges to better than 0.01% (Chantler et al. 2009), for X-ray $E1$ transitions. We have conducted studies of $E1$ visible transitions of the low-Z oxygen and confirmed convergence to 1% with a much smaller basis set (T. V. B. Nguyen et al., in preparation). Higher-order forbidden transitions are more sensitive to wavefunction overlap and to the wavefunction amplitude in narrow regions around the nucleus. We therefore conclude at this time that the $8.0\% \pm 2.3\%$ discrepancy remaining is yet due to incomplete wavefunctions in critical regions, and indeed that further work will be fruitful.

Where there are discrepancies between gauges it is of interest to query which gauge is more reliable. Grant & Starace (1975) suggested two approaches to interpreting the problem. The first approach, recommended by Starace, assumes that the model Hamiltonian is exact and then manipulated to be gauge invariant. This interpretation eventually leads to the conclusion that one should ignore the velocity gauge for calculations containing a non-local potential, such as Hartree–Fock, and to prefer the length gauge. On the other hand, Grant has stated that the inconsistency between the two gauges is an insight into a possible inaccuracy of the wavefunction. This implies that, in contrast to Starace's view, the model Hamiltonian may only be an approximation. Chantler and Froese-Fischer et al. (Froese-Fischer & Rubin 1998) believe that the energy denominator of the velocity gauge can lead to instability in the relativistic convergence.

5. DISCUSSION

Previous calculations listed in Table 1 were all based on non-relativistic techniques. The most advanced and most recent results of Froese-Fischer and Tachiev in 2004 ($I_{557.7}/I_{297.2} = 16.1$; Table 1) used LS coupling, following the

multi-configuration Hartree–Fock technique with Breit–Pauli corrections (MCHF+BP). In the low-Z regime, relativistic effects are relatively small, and LS coupling could in principle be sufficient to yield reasonable results. To apply the Breit–Pauli correction (or relativistic corrections) to the non-relativistic operators, the length gauge needs to be corrected only to order $O(\alpha^2)$. However, the velocity operator requires a correction to the gradient operator (Tachiev & Froese-Fischer 2002). Therefore, the results of Froese-Fischer and Tachiev were reported in the length gauge only. Our approach is able to compare relativistic results in both gauges and to obtain good convergence of different gauges. These are some of the main advantages of using this theory and GRASP2K for transition calculations.

Despite several key differences between our method and those of previous authors, our results in the length gauge for both cases ($I_{557.7}/I_{297.2} = 15.7$ for Method A and $I_{557.7}/I_{297.2} = 15.46$ for Method B) are relatively close to the recent results of Froese-Fischer and Tachiev ($I_{557.7}/I_{297.2} = 16.1$), who, as we have discussed, also reported their results in the length gauge. One could estimate that our result lies well within the uncertainty of the Froese-Fischer and Tachiev estimate. Our uncertainty in the convergence of the length gauge may be estimated to be quite small (± 0.03), but this does not exhaust possible systematic errors due to wavefunction incompleteness, especially in transition probabilities for forbidden transitions. It would be fair to estimate our final uncertainty as at least several percent as evinced by the 2.3% convergence step for A_V, and certainly considering the 8% gauge discrepancy, but A^L may possibly be accurate to 0.2%. In any case, our results are not consistent with the previous theoretical estimates within our own uncertainty.

More explicitly, our predictions are highly inconsistent with the recent spacecraft measurements in Table 3. Neither length nor velocity gauges agree with the results given by McConkey et al. (1966) and LeBlanc et al. (1966) as listed in Table 2 for laboratory experiments, nor with the airglow measurements. Although achieving a gauge convergence to within 8% for this particular $E2$ transition is by far the best in the literature, this raises key questions relating to the astrophysics and laboratory astrophysics. Why do the laboratory measurements not reproduce relativistic atomic theory within three standard errors? Are they reporting a dense or condensed system where particle interactions and collisions dominate? If so, how can these be addressed without loss of accuracy of the atomic processes?

Why are the airglow measurements so completely discordant with the theory and the laboratory measurements, and if one of them is shifted by pressure and density consideration why do they go in opposite directions? Given the quoted uncertainties of the experimental measurements, what type of systematic may not be accounted for in one of the two types of experiment?

Turning more broadly to the outstanding literature making use of the $E2$ transition as a marker and diagnostic, although obviously there is a marker based on the density of the excited state species, what limitation of validity of each of the models and conclusions is based upon the lack of clean normalization of the $E2$ signal? Rephrased, is the $E2/M1$ intensity ratio a constant, or a sensitive diagnostic functional needed for normalization of the signal in studies of planetary nebulae and meteor compositions (Halliday 1960; Jenniskens & Stenbaek-Nielsen 2004), meteoric aerothermal chemistry (Jenniskens et al. 2000), and direct correlation with disk accretion (Hartigan

et al. 1995)? How accurate are the modeling of atomic processes in comets such as the C/1996 B2 Hyakutake based on this green emission line (Bhardwaj & Raghuram 2012)? When the intensity variation of this emission line is used for studies of solar flare (Kudryashev & Avakyan 2000), the atmospheric system, and geophysical disturbances (Mikhalev 2011)? What systematic functional is involved in the divergence from an appropriate relativistic atomic model? These are just a few of the questions which this current study raises as a pointed question, but without at this time answering.

It is highly desirable to achieve a better convergence and a more reliable understanding of the processes occurring in stellar systems, in airglow and in laboratory experiments. The theory remains challenging. It should be kept in mind that the densities in which these experiments took place were relatively high, and it is possible that individual transition probabilities are affected by the pressure and the plasma environment. This could be explored systematically in laboratory astrophysical experiments, with higher accuracy airglow and stellar observations, and with additional theoretical challenges.

6. CONCLUSION

An in-depth analysis of the transitions $1s^2\,2s^2\,2p^4(^1S_0-^1D_2)$ and $1s^2\,2s^2\,2p^4(^1S_0-^3P_1)$ have been performed, where the transition probabilities were calculated using a fully relativistic MCDHF method. Results were reported in both the length and velocity gauges using two different methods of calculations with significantly different outcomes. We demonstrated that the success of a calculation relies strongly on the chosen configuration expansion methodology, but that the approaches fortunately yielded consistent outcomes but with different uncertainties. Our calculated intensity ratios appear to be in consonance with recent theoretical calculations, but with a well-defined uncertainty of perhaps a few percent based upon computational convergence in two gauges and by extrapolation. Our best estimate of the intensity ratio $I_{557.7}/I_{297.2} = 15.5$, based upon the length gauge. This is inconsistent with both the laboratory measurements and the airglow observations. It will be extremely valuable to characterize the experimental variation of the ratio under different plasma conditions and to compare that to observational measurements in different environments. Further theoretical work is also indicated.

REFERENCES

Baluja, K. L., & Zeippen, C. J. 1988, JPhB, 21, 1455
Bates, D. R. 1992, P&SS, 40, 893
Bhardwaj, A., & Raghuram, S. 2012, ApJ, 748, 13
Chantler, C. T., Hayward, A. C. L., & Grant, I. P. 2009, PhRvL, 103, 123002
Chantler, C. T., Lowe, J. A., & Grant, I. P. 2010, PhRvA, 82, 052505
Chantler, C. T., Lowe, J. A., & Grant, I. P. 2012, JPhB, 46, 015002
Condon, E. U. 1934, ApJ, 79, 217
Fischer, C. F., & Tachiev, G. 2004, ADNDT, 87, 1
Froese-Fischer, C., & Rubin, R. H. 1998, JPhB, 31, 1657
Froese-Fischer, C., & Saha, H. P. 1983, PhRvA, 28, 3169
Galavis, M. E., Mendoza, C., & Zeippen, C. 1997, A&AS, 123, 159
Garstang, R. H. 1951, MNRAS, 111, 115
Garstang, R. 1955, The Airglow and the Aurora (New York: Elsevier), 324
Gattinger, R. L., Lloyd, N. D., Bourassa, A. E., et al. 2009, CaJPh, 87, 1133
Gattinger, R. L., Vallance Jones, A., Degenstein, D. A., & Llewellyn, E. J. 2010, CaJPh, 88, 559
Grant, I. P., & Starace, A. F. 1975, JPhB, 8, 1999
Halliday, I. 1960, ApJ, 131, 25
Hartigan, P., Edwards, S., & Ghandour, L. 1995, ApJ, 452, 736
Jenniskens, P., Nugent, D., & Plane, J. M. C. 2000, EM&P, 82, 471
Jenniskens, P., & Stenbaek-Nielsen, H. C. 2004, AsBio, 4, 95
Jonsson, P., He, X., Froese-Fischer, C., & Grant, I. 2007, CoPhC, 177, 597
Kudryashev, G. S., & Avakyan, S. V. 2000, PCE, 25, 511
LeBlanc, F. J., Oldenberg, O., & Carleton, N. P. 1966, JChPh, 45, 2200
Lowe, J. A., Chantler, C. T., & Grant, I. P. 2010, PhLA, 374, 4756
Lowe, J. A., Chantler, C. T., & Grant, I. P. 2011, PhRvA, 83, 060501
McConkey, J. W., Burns, D. J., Moran, K. A., & Emeleus, K. G. 1966, PhL, 22, 416
Mikhalev, A. V. 2011, Ge&Ae, 51, 968
Mikhalev, A. 2012, Atmospheric and Oceanic Optics, 25, 224
Moore, C. E. 1993, Tables of Spectra of Hydrogen, Carbon, Nitrogen, and Oxygen (76th ed.; Boca Raton, Florida: CRC Press)
Pascucci, I., Sterzik, M., Alexander, R. D., et al. 2011, ApJ, 736, 13
Pasternack, S. 1940, ApJ, 92, 129
Russell, J. A. 1981, ApJ, 243, 317
Ryder, S., Staveley-Smith, L., Dopita, M., et al. 1993, ApJ, 416, 167
Semenov, A. I., & Shefov, N. N. 2005, Ge&Ae, 45, 797
Semenov, A. I., Shefov, N. N., Lysenko, E. V., Givishvili, G. V., & Tikhonov, A. V. 2002, PCE (Parts A/B/C), 27, 529
Sharp, W. E., & Siskind, D. E. 1989, GeoRL, 16, 1453
Shefov, N. N., Semenov, A. I., & Pertsev, N. N. 2000, PCEB, 25, 537
Slanger, T. G., Cosby, P. C., Huestis, D. L., & Bida, T. A. 2001, Sci, 291, 463
Slanger, T. G., Cosby, P. C., Sharpee, B. D., Minschwaner, K. R., & Siskind, D. E. 2006, JGR, 111, A12318
Stegman, J., & Murtagh, D. P. 1988, P&SS, 36, 927
Tachiev, G. I., & Froese-Fischer, C. 2002, A&A, 385, 716
Victor, G. A., Raymond, J. C., & Fox, J. L. 1994, ApJ, 435, 864
Witasse, O., & Nagy, A. F. 2006, P&SS, 54, 1381
Yamanouchi, T., & Horie, H. 1952, JPSJ, 7, 52